NGI Teknisk notat

Til:	Norges vassdrags- og energidirektorat
v/:	Aart Verhage
Kopi til:	
Dato:	2019-01-21
Rev.nr. / Rev.dato:	0/
Dokumentnr.:	20170131-08-TN
Prosjekt:	SP 4 FoU Snøskred
Prosjektleder:	Frode Sandersen
Utarbeidet av:	Dieter Issler
Kontrollert av:	

Dynamical Aspects of the 2017 Rigopiano Avalanche

Table of Contents

Sammendrag / ***Abstract***

Data on the disastrous snow avalanche that occurred on 2017-01-18 at the spa hotel Rigopiano, municipality of Farindola in the Abruzzo region of central Italy, are analyzed in the present Technical Note in different ways. The main results are the following:
(i) Avalanches in most other paths of this region appear to have run no farther than the β-point of their respective paths, but the 2017 Rigopiano avalanche went beyond the α-point predicted by the α-β model with standard Norwegian calibration.
(ii) The curvature and superelevation of the trimline between 1500 and 1300 m a.s.l. indicate that the velocity of the front was in the range 40–50 $\mathrm{m\,s^{-1}}$. In contrast, the tail velocity of the avalanche can hardly have exceeded 20 $\mathrm{m\,s^{-1}}$ in the same segment.
(iii) The deposits observed along all of the lower track and in the run-out zone lead to the conclusion that the avalanche eroded essentially the entire snow cover, but fully entrained only a moderate amount of snow (and debris). The entrainment appears to have had a considerable decelerating effect on the flow.
(iv) Estimates of the degree to which different parts of the building were damaged is combined with information about the location of the persons in the building and their fates. This allows to refine a preliminary vulnerability curve for persons in buildings that was based only on data from the 2015 Longyearbyen avalanche.

1 Introduction: Scope of this study

In the evening of January 18, 2017, a large snow avalanche released at about 1900 m a.s.l. on the east flank of Monte Siella in the municipality of Farindola in the Abruzzo region of Italy. Through the Grava dei Bruciati gully, it descended to the flat area called Rigopiano at 1100 m a.s.l. It completely destroyed the Hotel Rigopiano and killed 29 of the 40 persons waiting there for evacuation, making this the single most disastrous avalanche in Europe since 1970. The avalanche also destroyed or heavily damaged more than 5 ha of partly mature and partly young beech forest. At the time of writing, the judicial investigation of the event is still ongoing, and it may be expected that it will result in a major court case.

In early June 2017, the author surveyed the release area and track of this avalanche path, particularly with regard to the forest damage, and summarized the findings together with information retrieved from the Internet in the NGI Technical Note 20170131-02-TN (Issler, 2018), henceforth referred to as [I]. That survey revealed also that at least two further avalanches with long run-out occurred in the same period in the two adjacent paths to the north of the Grava dei Bruciati.

The aim of the present Technical Note is to elucidate the dynamics of this event in general terms, particularly with regard to the mass balance and the effect of the dense forest on the flow. It is planned to back-calculate this avalanche event with MoT-Voellmy and to compare our results with those obtained by Takeuchi and others (2018) for the 2008 event in the Makunosawa Valley, Japan in future work. In Sec. 2, we compare the run-out angles of several events in the Grava dei Bruciati path and three other nearby paths, for which there is sufficient historical information, with the α-β topographical-statistical model (Lied and Bakkehøi, 1980; Lied and Toppe, 1989). Next, the curvature and superelevation of the flow as inferred from the trimlines in the middle to lower track are used to estimate the velocities of both the fast front and the slow tail of the Rigopiano avalanche (Sec. 3), in a similar way as was done by Issler and others (2008) for avalanches observed in Switzerland in 2006. In Sec. 4, the qualitative information available from drone videos during the aftermath of the avalanche is used to constrain the evolution of the mass balance along the Grava dei Bruciati path. These estimates can then be used in the momentum balance of the avalanche to assess the importance of entrainment and to differentiate between snow (and debris) that was fully entrained into the flow on the one hand, and material that merely was dragged along for a limited distance on the other hand. In Sec. 5, we estimate the impact pressure generated by the avalanche and compare it to the pressures that trees can be expected to sustain. The large number of persons involved in this catastrophe and sufficient information on the degree of damage at their respective locations allows an update of the vulnerability curve derived from the 2015 Longyearbyen avalanche (Issler and others, 2016b), see Sec. 6. The conclusions in Sec. 7 discuss how field observations like the ones at Rigopiano can test the adequacy of present-day flow models with simple friction laws and entrainment and obstacle-drag formulas.

2 Comparison with a topographical-statistical run-out model

As detailed in [I], some information on the run-out distances of frequent as well as rare avalanches can be inferred from historical sources, aerial photos and our survey observations for the Grava dei Bruciati path and four other paths in the vicinity. The reach of avalanches with return periods of approximately ten years is discernible as the boundary of dense forest consisting of shrubs and very young, flexible trees.

At the time of the field survey, the run-out area around the destroyed Hotel Rigopiano was closed off by the authorities so that we could not determine the run-out distance of the 2017 avalanche directly. However, debris visible in Fig. 12 of [I] indicates that the horizontally measured run-out distance from the probable fracture line is around 2200 m. It is unclear, however, whether the debris visible in the photo was deposited by the dense/fluidized part of the avalanche or carried by the powder-snow cloud.

Extensive statistical analysis of data from rare to extreme avalanches suggests that the run-out angle α is highly correlated to the average path steepness β—at least for reasonably smooth, parabola-like path profiles (Lied and Bakkehøi, 1980; Lied and Toppe, 1989). α is measured from the fracture crown to the toe of the deposit following the path, β is the angle from the fracture crown to the point where the path inclination drops below 10°. For several regions (Norway, Tyrol, coastal British Columbia), linear correlations

Table 1 Path steepness β, observed run-out angle α, and expected run-out angle for an extreme avalanche event according to the α-β model calibrated on avalanches from western Norway. Angles are rounded to nearest degree. Values for the 1959 avalanche in Grava dei Bruciati are rough estimates. The values for avalanches with return period of approximately 10 years are estimated from the extent of stands of bushes and very young trees near the centerline of the path.

Avalanche path	Date	Drop height	Run-out	Path steepness β	α-angle observed	α-angle predicted
Grava di Valle Savina	2017	675 m	1200 m	29°	29°	27°
Grava di Valle Cupa	~10 y	500 m	890 m	26°	29°	23°
	2017	590 m	1125 m	26°	28°	23°
Grava di Costa Mercante	~10 y	380 m	580 m	28°	33°	26°
	2017	550 m	1000 m	28°	30°	26°
Grava dei Bruciati	~10 y	425 m	700 m	22°	31°	20°
	1959	735 m	1900 m	22°	21°	20°
	2017	770 m	2190 m	22°	19°	20°
Monte San Vito	1963	1165 m	2470 m	26°	25°	24°
	2014	560 m	1120 m	26°	26°	24°

between α and β (Lied and Bakkehøi, 1980) have been established for avalanche events with long return periods. For western Norway, the correlation is $\alpha = 0.96\beta - 1.4°$, with a standard deviation of 2.3°. It is instructive to check whether this relation also holds for avalanches in the Gran Sasso area.

In Table 1, α and β are estimated for known events in several avalanche paths. Both angles were determined manually from a printed topographic map at a scale of 1:16,667. In particular, the β point was not determined from a parabolic interpolation of the path, but estimated from the contour lines; the uncertainty in its location is of the order of 50 m. In most cases, the location of the fracture line had to be guessed. Accordingly, the uncertainties in α and β are considerable.

Of the seven recorded avalanche events in five paths, about half stopped at or above the β point; only the exceptionally long 1963 avalanche from Monte San Vito and the two recorded Rigopiano avalanches exceeded the β point. The 2017 Rigopiano event is the only one to go beyond the α point expected from the Norwegian correlation. This raises the question whether these relatively short run-out distances are primarily due to the braking effect of the forest—which is more pronounced for small avalanches than for large ones—or whether the statistical correlation between α and β for the Gran Sasso region differs significantly from the one obtained for rare avalanche events in western Norway. We plan to come back to this point in a future publication, where we compare simulations accounting for forest drag with simulations disregarding it.

Figure 1 The ridge at 1500 m a.s.l., from the northern rim above the gully. Note the strong curvature of the trajectory across the ridge line and the complete desctruction of the forest on the downward slope

3 Velocity estimates

Four observations can be used to obtain rough estimates of the velocity of the head and the tail of the 2017 avalanche in the middle to lower track: (i) Parts of the avalanche overflowed the terrain shoulder at 1500 m a.s.l. with little deflection (Figs. 1 and 2). (ii) In the left bend at 1300 m a.s.l., the trimline is 30–40 m above the gully floor and has a radius close to 300 m. (iii) The shoulder deflected the tail of the avalanche, which circled around its foot with a curvature radius of no more than 100 m. (iv) Similarly, in the left bend at 1300 m a.s.l., debris was deposited along the thalweg while trees only 5–10 m away were left unscathed. The minimum curvature radius of the flow was about 90 m.

Avalanche flow in complex terrain is a three-dimensional problem that needs to be drastically simplified in order to obtain velocity estimates without detailed numerical simulations. We will disregard a potential powder-snow cloud and follow the motion of a reasonably small columnar element in the avalanche, its height being equal to the local depth of the dense or fluidized layer. We treat it as a mass point, but keep in mind that there may be forces due to earth pressure. Another important simplification is to assume that the bed friction and the down-slope gravitational force balance approximately along the main path, except for some distance downstream of pronounced path inclination changes. This means that these two opposing forces drop out of the momentum balance

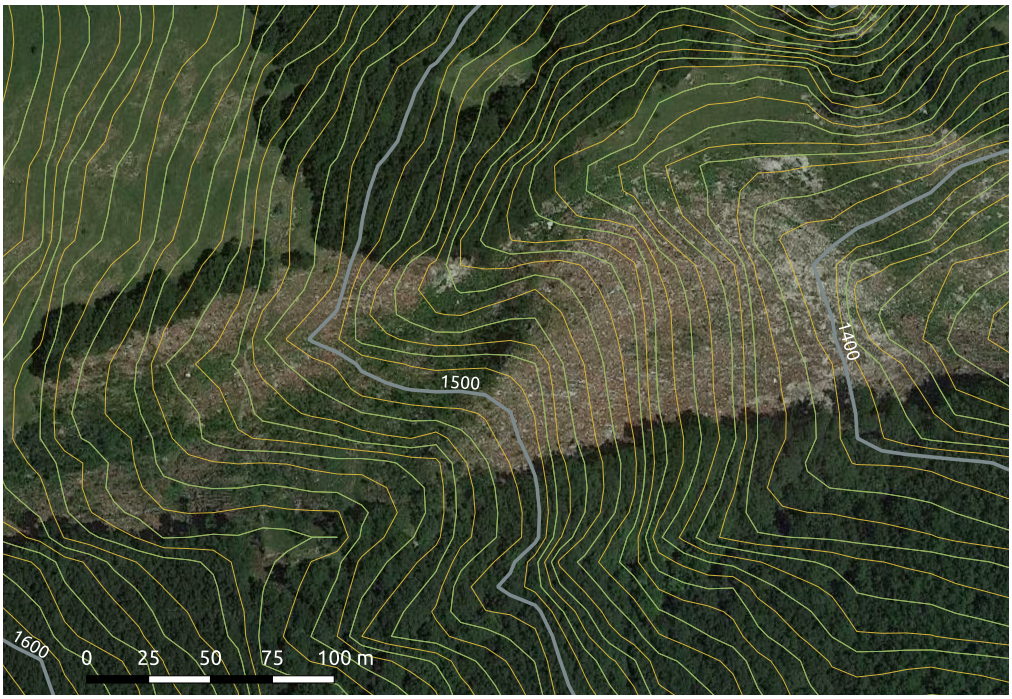

Figure 2 Detail of Fig. 3 in [I], showing the pronounced shoulder at 1500 m a.s.l. after the 2017 avalanche. Equidistance of isolines 5 m

except where the avalanche trajectory deviates considerably from the path of steepest descent. This is the case at the ridge at 1500 m a.s.l., which was overflowed by the front of the avalanche, and in the left bend at 1300 m a.s.l., where the trimline is far above the gully floor. In these cases, we should take into account a term $g(\sin\theta - \sin\theta_{\mathrm{PSD}})$ in the equation of motion, with θ_{PSD} the inclination along the path of steepest descent along the gully floor.

The simplest situation to analyze is the trajectory across the shoulder in Fig. 2 along the southern trim line. We can get a lower bound on the velocity by noting that the avalanche front crossed the ridge and retained enough speed to cut down any tree that was not flexible (this includes more or less all the trees on the eastern slope). From the isolines derived from the DEM, and shown in Fig. 2, one infers that the avalanche did not have to climb a counterslope, but was $\Delta H \approx 15\,\mathrm{m}$ higher at the crest of the ridge than if it had taken a trajectory towards the narrow port of the gully. However, the photo in Fig. 1 (confirmed by the author when he climbed that ridge during the survey) shows clearly that the avalanche had to ascend a counterslope and that the altitude difference ΔH between the two trajectories was closer to 30 m. We estimate that the velocity had to be at least $v_2 = 20\text{–}25\,\mathrm{m\,s^{-1}}$ at the top of the ridge for the avalanche to completely destroy the forest on the downslope. A simple energy balance then gives the approach velocity v_1 as

$$\frac{1}{2}v_1^2 \approx \frac{1}{2}v_2^2 + g\Delta H. \tag{1}$$

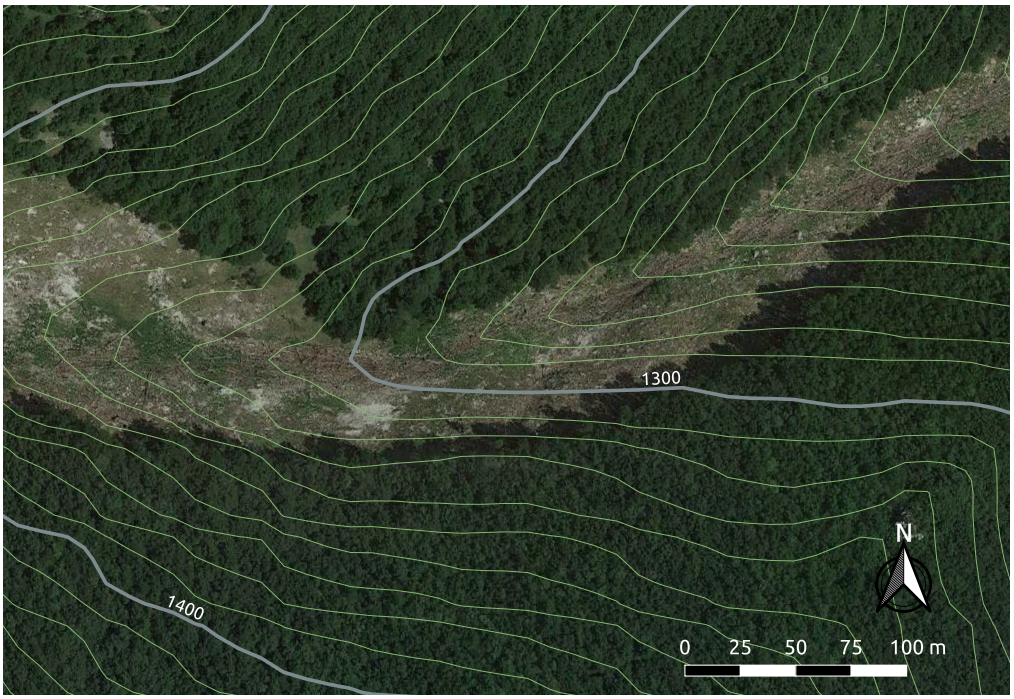

Figure 3 Detail from satellite image Fig. 3 in [I] around the left bend at 1300 m a.s.l. after the 2017 avalanche event. The trimline is at the transition from light foliage to dark green shadows. Equidistance of isolines 10 m

(Recall that ΔH is relative to a trajectory for which the downslope gravitational acceleration and friction balance.) Using $\Delta H = 15$ m from the DEM, we find $v_1 \geq 26$–$30\,\mathrm{m\,s^{-1}}$, whereas $\Delta H = 30$ m leads to $v_1 \geq 32$–$35\,\mathrm{m\,s^{-1}}$.

The ridge being rather sharp with an estimated curvature radius of no more than 20 m, an avalanche reaching the top with a speed above $15\,\mathrm{m\,s^{-1}}$ will lift off and jump some distance over the ridge. We neglect air resistance and assume the avalanche lifts off near the top of the ridge with a speed v_2 under an angle θ_2 from the horizontal, whereas the downslope inclination is θ_3. The horizontal jump distance then becomes

$$x_{\mathrm{jump}} \approx \frac{v_2^2}{g}\left[[1+\cos(2\theta_2)]\tan\theta_3 + \sin(2\theta_2)\right]. \qquad (2)$$

The average downslope inclination is $\theta_3 \approx 37°$, while one may assume $0° < \theta_2 < 30°$. In this range, $1.5v_2^2/g < x_{\mathrm{jump}} \leq 2v_2^2/g$. Given the length of the downslope, one may safely assume that $x_{\mathrm{jump}} < 100$ m, which leads to an upper limit of $v_{2,f} < 22$–$26\,\mathrm{m\,s^{-1}}$. Despite the considerable uncertainties of our simplified treatment of the problem, we can thus conclude that the approach velocity of the outer edge of the avalanche front should have been near 30–$35\,\mathrm{m\,s^{-1}}$. Much of the forest on the downslope side of the ridge was destroyed *after* the passage of the front, when the approach velocity was 20–$25\,\mathrm{m\,s^{-1}}$.

In analyzing the information contained in the trim line at the left bend, one first needs

to account for the general inclination of the path, which is $\theta \approx 20°$ in this area. As a result, the true curvature of the trajectory along the trim line is reduced by a factor $\cos^2 20° \approx 0.88$, i.e., the curvature radius, R, is 300–330 m. We will use a coordinate system where the x-axis is along the flow direction, i.e., inclined to the horizontal by the angle θ, the y-axis is horizontal, normal to the x-axis and pointing towards the center of the osculating circle, while the z-axis is normal to both x and y and inclined by the angle θ relative to the vertical. If we neglect friction and the transverse earth pressure gradient, there has to be approximate balance between the z-component of gravity and the z-component of the normal force exerted by the gully embankment, while the horizontal component of the normal force has to equal the centripetal force:

$$a_{n,z} = a_n \cos\theta \cos\psi = -g_z = g\cos\theta,$$
$$a_{n,y} = a_n \cos\theta \sin\psi = a_{\mathrm{cp}} = v_f^2/R,$$

where $\psi = 30$–$40°$ is the slope angle of the embankment. From this we obtain a first rough estimate of the front velocity along the trim line:

$$v_f \approx \sqrt{Rg \tan\psi / \cos\psi} \approx 40\text{–}50\ \mathrm{m\,s^{-1}}.$$

Two important effects have been neglected in this analysis, however: First, friction forces transverse to the direction of motion do not affect the momentum balance in the longitudinal direction (x), but they enter the quasi-static equilibrium formulated above. The corresponding force per unit mass in the y-z-plane is $-b(z)\mu a_n$, where $b(z)$ is unknown, but in the range $[-1, +1]$; its z-component is $b(z)\mu a_n \sin\psi \cos\theta$ and its y-component is $-b(z)\mu a_n \cos\psi \cos\theta$. Second, pressure forces transverse to the flow direction arise because the masses flowing near the valley centerline will have similar velocity as those along the trim line, but the curvature radius is about three times smaller and the centripetal force accordingly about three times larger. For the sake of simplicity, we assume that the flow depth and velocity are independent of $R(z)$ so that $a_z(z) = v_f^2/R(z)$. We set $R(z) \approx R_1 + (R_2 - R_1)z/\Delta H$, where $R_1 \approx 100$ m, $R_2 \approx 300$ m and $H \approx 40$ m. We denote the transverse gradient of the depth-averaged pressure per unit mass (units $\mathrm{m\,s^{-2}}$) by $\hat{p}'(z)$, with components $\hat{p}'_y(z) = -\hat{p}'(z)\cos\psi$ and $\hat{p}'_z(z) = \hat{p}'(z)\sin\psi$. With this, the equilibrium conditions above can be formulated as

$$a_n(z)[\sin\psi - b(z)\mu\cos\psi] + \hat{p}'(z)\cos\psi = a_z(z), \quad (3)$$
$$a_n(z)[\cos\psi + b(z)\mu\sin\psi] - \hat{p}'(z)\sin\psi = g. \quad (4)$$

There are three unknown functions $a_n(z)$, $b(z)$ and $\hat{p}'(z)$ and an unknown number (u_f within $a_z(z)$), but only two equations for each value of z. It is plausible that the lateral borders of the avalanche are not supported by any obstacle or counterslope, so that $\hat{p}(0) = \hat{p}(H) = 0$. Then we can eliminate the unknown pressure gradient term by integrating over z, leaving us with two equations for the three unknowns $A_n \equiv \int_0^H a_n(z)\mathrm{d}z$, $BA_n \equiv \int_0^H a_n(z)b(z)\mathrm{d}z$ and v_f^2. With $-1 \le b(z) \le +1$ and $\mu\cos\psi < \sin\psi$, we can obtain upper and lower bounds by assuming a value for B and varying that value. Moreover, it may well be that $b(z) < 0$ near $z = 0$ and $b(z) > 0$ near $z = H$,

which would make $|B| \ll 1$. The approximation for $R(z)$ gives $A_z \equiv \int_0^H a_n(z)\mathrm{d}z = v_f^2 H/(R_2 - R_1)\ln(R_2/R_1) \approx 0.22 v_f^2$. From this, the following formula results:

$$v_f \approx \sqrt{\frac{gH}{\ln(R_2/R_1)} \cdot \frac{\sin\psi - \mu B\cos\psi}{\cos\psi + \mu B \sin\psi}}. \tag{5}$$

With $\psi = 35°$, H = 30–40 m, $R_1 = 100$ m, $R_2 = 300$ m, μ = 0.3–0.5 and $-0.5 \le B \le +0.2$, v_f lies in the range 28–46 m s^{-1}, the most probable range being 35–40 m s^{-1}.

Finally, we consider whether constraints on the velocity can be inferred from the pronounced bend below 1430 m a.s.l., at the foot of the shoulder discussed above. The gully widens, and the thalweg makes a right turn through an angle of approximately 90° with a radius of about 90 m. The slope on the outer side of the thalweg has variable inclination, with 35° a typical value in its northern part. The radius of the osculating circle at the outer edge of the flow is 100–110 m. When trying to obtain simple velocity estimates, one has to keep in mind that only relatively slow parts of the avalanching mass could follow this trajectory because they had to make a sharp left turn at 1530–1500 m a.s.l. The flow should, however, still be supercritical; hence, we assume that the strong confluence of the masses flowing around the shoulder and those flowing over it does not influence the flow in the bend at 1450–1410 m a.s.l. We apply again Eq. (5), setting $H = 25$ m, $R_1 = 60$ m, $R_2 = 110$ m and $\psi = 35°$ as central values. Assuming $0.3 \le \mu \le 0.5$ and $-0.5 \le B \le +0.2$ as before, we obtain mean velocities in the range $15\,\mathrm{m\,s^{-1}} < \bar{v} < 22\,\mathrm{m\,s^{-1}}$.

4 Reconstruction of the mass balance

The release volume is estimated to have been in the range 75,000–160,000 m^3, corresponding to a mass in the range 10–40 kt if the slab density is assumed in the range 150–250 $kg\,m^{-3}$ [I, Sec. 3.1]. In the following, we shall use central values of 120,000 m^3 and 25 kt, respectively.

We do not precisely know the extent of the deposits and have only qualitative information on the deposit depth. It appears plausible that uprooted trees stopped and held back a considerable amount of avalanche snow when they came to a stop. From around 1550 m a.s.l. to 1250 m a.s.l., tree debris is concentrated on the gully floor; this area has (projected) length of approx. 850 m and an average estimated width of at least 20–30 m. It appears fair to assume that the deposit depth was at least 1 m due to the roughness created by the tree debris and that the deposit density was in the range 300–500 $kg\,m^{-3}$. This gives a lower bound of 5–12 kt of deposited snow, but the actual value could exceed 30 kt since the deposit may have been deeper—photos and videos from the rescue operation indicate that the tree debris were not visible for some time after the event (this was helped by the snowfall continuing after the avalanche descent).

From the end of the Grava dei Bruciati to the distal end of the deposit, the horizontal distance is about 750 m. Figure 12 in [I] suggests that the deposit beyond the gully had approximately oval or rhomboidal shape, with a maximum width of about 100 m. This amounts to an area of 40–55,000 m^2. The average deposit depth in this area is at least 2 m and perhaps as much as 5 m since the debris of the four-story hotel was mostly covered by snow. The difficulties of digging the victims out indicates that the snow was very hard, with a density presumably in the range 400–500 $kg\,m^{-3}$, to judge from experience with other large avalanches (Issler and others, 2016a). From this, we estimate a deposit mass in the range 35–100 kt in the run-out area. Combining the track and the run-out area, we see that the deposit mass exceeded the release mass by 0–120 kt or by a factor of 1–12. The most likely values are 70–80 kt, i.e., a gain by a factor 3–4.

The area overflowed by the avalanche (excluding the release area) amounts to approximately 200,000 m^2. This implies that about 350–400 $kg\,m^{-2}$ of snow (or a snow water equivalent of 350–400 mm) were mobilized on average. This is more than the new-snow sum of the days before the disaster and would imply that a substantial part of the old snow cover also was eroded. This is perhaps less surprising than it might appear at first: When trees are uprooted, their root system acts like a snow plow so that one should, in fact, expect most of the snow cover to be mobilized.

An interesting and relevant question is to which degree these snow masses were not just eroded, but properly entrained into the avalanche flow, and how far the eroded snow traveled on average. Sovilla and others (2001) dug a large number of transverse snow pits along the Monte Pizzac avalanche path and so were able to determine the total mass flux across the cross-section, $M(x)$, the total erosion per unit length, $E(x)$, and the total deposition per unit length, $D(x)$, as functions of the coordinate along the path, x.

Such information is invaluable for testing advanced erosion/deposition models and is not available from LiDaR scans or photogrammetry before and after the avalanche event. A detailed reconstruction of $M(x)$, $E(x)$ and $D(x)$ is obviously not possible for this event, but the observations summarized above imply the following:

- Both $E(x)$ and $D(x)$ are large, and to first approximation $D(x) \lesssim E(x) \approx \bar{\rho}_s(x)\bar{H}_S(x)W(x)$, where $\bar{\rho}_s$ is the average snow-cover depth at x, $W(x)$ is the width of the avalanche path, and $\bar{H}_S(x)$ is the snow-cover depth averaged over the width.

- There is no observational information about erosion and deposition in the upper track above around 1550 m a.s.l., but based on experience from other avalanche paths (Monte Pizzac, Vallée de la Sionne, Ryggfonn), it is likely that $D(x) \gtrsim 0$ while the net entrainment rate probably was almost equal to the erosion rate so that $M(x)$ increased rapidly in that path segment.

- The deposited mass in the run-out area below 1200 m a.s.l. appears to be significantly larger than the mass of the snow cover before the avalanche. Hopefully, this statement can be made semi-quantitative when data from the official site investigation becomes available. It appears likely, however, that the mass of the deposited snow exceeds the release mass, implying that $E(x) > D(x)$ at least in the steeper parts of the path down to perhaps 1400 m a.s.l.

- Detailed measurements at Vallée de la Sionne as well as dynamical considerations indicate that deposition occurs only in the tail of an avalanche, except right before it stops. This suggests that much of the fully entrained snow—possibly stemming from the upper layers of the snow cover—traveled over a large distance, whereas older snow from near the ground was dragged along a relatively short distance and deposited as the tail of the avalanche passed over it.

- On the one hand, substantial masses of tree debris were deposited near the distal end of the avalanche, where there had been no forest. This implies that some trees were dragged at least 200–300 m by the avalanche. On the other hand, uprooted or broken trees can be found a short distance below the point where the avalanche entered the forest. This can be taken as evidence that the tree destruction rate (the number or mass of trees per unit area that were broken and/or uprooted) exceeds the debris deposition mass per unit area at least in the steeper reaches of the path.

The inferences mentioned above are graphically summarized in Fig. 4 in a form that can be compared to the plots of the measurements by Sovilla and others (2001). Since there are no measurements from the Rigopiano avalanche, Fig. 4 ĩs only one possible scenario among many. The example shown has a release mass slightly below 20 kt and the mass flowing through a cross-section peaks at close to 40 kt. Developing such scenarios is useful for understanding the limitations that the characteristics of the avalanche path impose on the mass balance. In particular, the spatial erosion rate $e(x)$ is limited by the

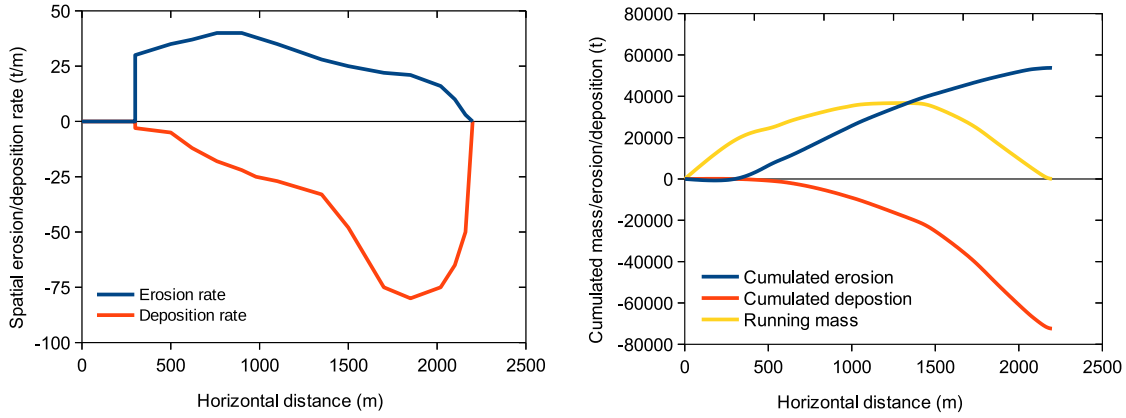

Figure 4 Left panel: Qualitative representation of the spatial erosion rate $e(x)$ and the spatial deposition rate $d(x)$. Right panel: Evolution of $M(x)$, the mass passing the cross-section at x, the accumulated erosion, $E(x) = \int_{x_{sw}}^{x} e(x')\mathrm{d}x'$, and the accumulated deposition, $D(x) = \int_{x_{sw}}^{x} d(x')\mathrm{d}x'$. x_{sw} is the location of the stauchwall. Note that $M(x_{sw}) + E(x) + D(x) = M(x)$. These diagrams are patterned after the presentation of the measurements from Monte Pizzac by Sovilla and others (2001), but are not based on actual measurements

width of the gully and the total snow depth; in order to reproduce the large deposited mass in the run-out area below 1200 m a.s.l. and the substantial deposition above that altitude, one has to assume that essentially all snow in the avalanche track was eroded. The erosion and deposition rate shown in the figure does not include the mass of the broken or uprooted trees, which would contribute in the same order of magnitude as the snow.

An indication of the degree to which the avalanche was able to *entrain* the snow and the trees can be obtained by considering the momentum balance of the entire avalanche. If its mass and mean velocity are $M(t)$ and $v(t)$, respectively, the total momentum is $J(t) = M(t)v(t)$, the down-slope gravitational force is $F_g = M(t)g\sin\theta(t)$. To accelerate the eroded snow (and tree debris) to the speed $v(t)$, momentum has to be transferred at a rate $\mathrm{d}J_e/\mathrm{d}t = e(x(t))v^2(t)$. With the ranges 20–40 kt for $M(t)$, 0.2–0.7 for $\sin\bar{\theta}$, 20–40 t m^{-1} for $e(t)$ and 30–50 m s^{-1} for $v(t)$, one finds $F_r = (0.4 \ldots 2.8)\times 10^8$ kg m s^{-2} and $\mathrm{d}J_e/\mathrm{d}t = (0.2 \ldots 1.0)\times 10^8$ kg m s^{-2}. A substantial part of the gravitational traction is expended against friction between the entrained layer and the residual snow cover. Taking these considerations together, we conclude that complete entrainment of the eroded snow cover is barely possible in steep reaches of the avalanche path and that much of the eroded snow and tree debris can only be dragged along at low speed in the more gently inclined lower reaches. Despite their crudeness, our estimates appear to be well confirmed by the observations.

5 Observational limits on impact pressure

5.1 Limits inferred from forest destruction

Information from trimlines Except for small islands in the upper track that are sheltered to some degree by topographical features, the forest was essentially completely destroyed wherever the avalanche reached. An exception are the lateral edges of the path where the flow is stopped a few meters inside the surviving forest without producing much damage. This is best exemplified in Fig. 25 of [I], but can also be observed by enlarging Figs. 12, 16, 18 and 21. Such a damage pattern can be explained if (i) the impact pressure of the avalanche along the trimline was close to the minimum value, p_{thr}, for breaking or uprooting the trees, (ii) the pressure rapidly diminished farther away from the centerline, and (iii) there were no pronounced variations of p_{thr} along the flow direction of the avalanche.

If the three suppositions above are correct, knowing p_{thr} will only give us information on the maximum impact pressure along two lines in the flow domain. In particular, the question remains unanswered whether the pressure is much larger close to the centerline of the flow. Nevertheless, an estimate of the pressure needed to break or uproot an average tree will be useful in understanding how much kinetic energy of the avalanche is dissipated as the forest is being destroyed.

Breakage vs. uprooting While some trees were broken or both uprooted and broken, the majority were only uprooted. There are variations in strength between tree specimens of the same kind, age and girth due to local variations in growth conditions. It would, however, not be correct to conclude that the avalanche pressure was such that the resulting bending moments were just above the lower limit for breakage of beech trees. Rather, one may conclude that root systems of the trees could sustain less bending moment than the trunks; moreover, if the root system failed quickly, the bending moment was reduced significantly as the trees toppled, explaining why most trees were not broken. The strength of the bond between tree roots and ground should be expected to vary even more than trunk strength. Such variation may explain why some trees were broken but not uprooted.

Minimum avalanche pressure for breaking trees A tree trunk breaks when either the tensile stress near the outer periphery of the trunk or the compressive stress near the inner periphery exceed the modulus of rupture (MOR). The MOR has been measured by many authors, with somewhat differing results; in particular, it is about 50% higher for dried wood than for green wood. According to (Forest Products Laboratory, 1999, ch. 4), the MOR for (green) beech is about 59 MPa. With some simplifying assumptions of homogeneity across the cross-section, the maximum bending moment can be obtained by integration across the cross-section:

$$M_{b,\max} = \frac{\pi}{32}\,\text{MOR}\,d^3 \approx (5\text{–}6\,\text{MPa})\,d^3, \tag{6}$$

Figure 5 View of the hotel before the 2017 avalanche. The original cabin Rifugio Tito Acerbo (small grey stone structure to the right) was integrated into the much larger new building. Note the dense forest along the avalanche track. Image from the website `https://geograficamente.wordpress.com/2017/01/30/il-duro-inverno-dellappennino-centrale-terremoto-neve-valanghe-e-impreparazione-agli-eventi-naturali-in-mano-alleroismo-di-pochi-il-caso-dellhotel-rigopiano-e-il-per/`*, retrieved on 2017-09-01*

where d is the trunk diameter at the failing cross-section. For simplicity, d is often replaced by the diameter at breast height (DBH). A beech with $d = 0.2\,\mathrm{m}$ will thus break at a bending moment of 40–50 kN m, whereas 600–750 kN m are required to break one with $d = 0.5\,\mathrm{m}$.

To estimate the bending moment due to an avalanche, we assume a local slope angle θ, a snow depth h_s and a flow depth h_f (both measured normal to the ground), flow density ρ_f, flow velocity profile $u(z)$ (with z the coordinate normal to the ground), and a constant trunk diameter d. For simplicity, we neglect drag forces along the axis of the tree trunk, due to the oblique impact, and apply a drag formula that is appropriate for flow of cohesionless granular materials around a cylinder: (Chehata and others, 2003; Wassgren and others, 2003; Issler and others, 2019):

$$C_D \approx 1 + 5\mathrm{Fr}^{-2}, \tag{7}$$

with $\mathrm{Fr} \equiv \bar{u}/\sqrt{h_f g \cos\theta}$. Then we obtain

$$M_b = \frac{1}{2}\left(1 + \frac{5gh_f \cos\theta}{\bar{u}^2}\right)\rho_f d \int_{h_s}^{h_s+h_f} z u^2(z)\mathrm{d}z \cos^2\theta. \tag{8}$$

The integral evaluates to

$\left(\frac{h_s}{h_f} + \frac{1}{2}\right)h_f^2\bar{u}^2$ for a uniform profile $u(z) = \bar{u}$,

$\left(\frac{6h_s}{5h_f} + \frac{33}{40}\right)h_f^2\bar{u}^2$ for a Newtonian profile $u(z) = \frac{3}{2}\bar{u}\left[1 - \left(1 - \frac{z}{h_f}\right)^2\right]$,

$\left(\frac{5h_s}{4h_f} + \frac{25}{28}\right)h_f^2\bar{u}^2$ for a Bagnold profile $u(z) = \frac{5}{3}\bar{u}\left[1 - \left(1 - \frac{z}{h_f}\right)^{3/2}\right]$,

$\left(\frac{4h_s}{3h_f} + 1\right)h_f^2\bar{u}^2$ for a linear profile $u(z) = 2\bar{u}\frac{z}{h_f}$.

Our lack of knowledge of the velocity profile leads to an uncertainty of about $\pm 30\%$, and the effect of a non-uniform density profile has not been accounted for in this simple analysis. For plausible values $1/3 < h_s/h_f < 1/2$, the integral is in the range 0.8–1.7. With typical Froude numbers in the range 3–7, one has $1.6 > C_D > 1.1$, so that we estimate

$$M_b \approx (1\text{–}3)h_f^2 d \cos^2\theta \cdot \frac{1}{2}\rho_f \bar{u}_f^2. \tag{9}$$

Comparing Eq. (8) to Eq. (6), we find the following criterion for the stagnation pressure $\frac{1}{2}\rho_f\bar{u}_f^2$ that will break beech trees:

$$\bar{p}_{\mathrm{stag}} > (3\text{–}10)\,\mathrm{MPa}\,\frac{d^2}{h_f^2}. \tag{10}$$

If we assume $h_f \approx 2\,\mathrm{m}$, young trees with $d = 0.2\,\mathrm{m}$ will break at stagnation pressures of 30–100 kPa, while 120–400 kPa are needed for mature trees with $d = 0.4\,\mathrm{m}$. The

majority of trees in the avalanche path likely had trunk diameters of 0.3 m or less, so stagnation pressures of 70–200 kPa would have been able to break their trunks. The velocity estimates of Sec. 3 lead to stagnation pressures in the range 50–150 kPa. One may therefore expect that some of the oldest trees in favorable locations could have withstood the avalanche if their root system provided sufficient anchoring and if they were not felled by the impact of uprooted trees swept along by the avalanche.

Minimum avalanche pressure for uprooting trees A bending moment applied to the tree trunk is transmitted to the root system as long as the trunk does not break. According to the field observations, the failure surface of the root system can be approximated quite well by a hemisphere with a diameter in the range 1.5–3 m. The soil layer is very shallow in the Grava dei Bruciati, but the karstic limestone is heavily weathered so that the beech roots penetrated into it and significant masses of rocks were pulled out together with the roots. The resistance against the bending moment can therefore be attributed to the shear strength of both the roots and the weathered bedrock.

Assuming for simplicity that the shear strength of the root–soil system has a constant value τ_r along the hemispherical failure surface with diameter D, the moment at failure is

$$M_{r,\max} = \frac{\pi^2}{16}\tau_r D^3. \tag{11}$$

Comparing this with Eq. (6), we find that a tree is uprooted rather than broken if

$$\tau_r < \frac{1}{2\pi}\mathrm{MOR}\left(\frac{d}{D}\right)^3. \tag{12}$$

According to the observations described in [I], most trees were uprooted and $D < 10d$, Mattheck and others (2003, Fig. 14) indicate $D = 5\text{–}7d$ for trees in dense stands. With the latter values, we obtain an upper limit $\tau_r < 30\text{–}80$ kPa for the shear strength of the soil–root system. This appears plausible for this type of soil. Unfortunately, we do not have other, independent ways of estimating the soil shear strength in this location, such as pulling tests on trees.

An experimental study on tree resistance in the central Amazon basin (Ribeiro and others, 2016) found critical bending moments in the range 50–400 kN m for different tree species with BHD from 0.2 to 0.4 m, but on average $M_{b,\max}$ seemed to increase about linearly with BHD, rather than with the third power as predicted by the simple mechanical analysis. Moreover, they found comparable numbers of failure due to snapping and uprooting, with some variations between species and type of terrain.

Energetics of forest destruction As long as a tree remains standing in an avalanche flow, it dissipates flow energy at the rate $P_{t,\mathrm{drag}} = F_t\bar{u}$, where F_t is the force acting on the tree. While the tree is falling and accelerating, it extracts further energy from the flow, but dissipates only part of it and increases its kinetic energy. Once it has attained the flow speed of the avalanche, it continues to dissipate energy—mainly by adding to the bed friction of the avalanche—at the rate $P_{t\,\mathrm{fric}} = \mu_{\mathrm{eff}}(m_t, \bar{u})m_t g\bar{u}\cos\theta$, m_t being the

average mass of a tree. At the same time, the tree converts potential energy to kinetic energy at the rate $P_{t\,\mathrm{grav}} = m_t g \bar{u} \sin\theta$ as it is rafted down-slope. In sufficiently steep terrain, the flow velocity will tend towards the value $\bar{u}_{\mathrm{eq}}$ for which

$$Mg(\sin\theta - \mu_{\mathrm{eff}} \cos\theta) - N_t F_t - \dot{M}\bar{u}_{\mathrm{eq}} = 0.$$

N_t is the number of standing trees inside the flow and varies with time. M, the mass of the avalanche, also changes with time due to entrainment and deposition of both snow and tree debris. From this, one obtains the equilibrium velocity as

$$\bar{u}_{\mathrm{eq}} = \frac{Mg(\sin\theta - \mu_{\mathrm{eff}} \cos\theta) - N_t F_t}{\dot{M}}. \tag{13}$$

The mass growth rate can be estimated as

$$\dot{M} \approx (n m_t + \rho_{sc} h_{ne}) B \bar{u}, \tag{14}$$

with $n \cos\theta$ the stand density, corrected for the obliquity of the terrain, B the width of the avalanche, ρ_{sc} the snow-cover density, and h_{ne} the net entrainment depth (or the erosion depth minus the deposition depth corrected for density change). In the case of the 2017 Rigopiano avalanche, N_t is the product of $n \cos\theta$, B, and the mean length of the tree destruction zone at the avalanche front. Except for the latter quantity, we can make reasonable assumptions about the values of these variables based on observations.

These considerations show that the over-all dynamics of an avalanche flowing through a forest depends sensitively on how long the trees can withstand the pressure from the avalanche and exert a braking force. or, phrased differently, how much energy they can absorb until they fail. The time until breaking or uprooting cannot be straightforwardly calculated from the modulus of rupture of the tree or from the failure moment of the root system because the load history and maximum deformation from impact to extraction of the tree are not known.

An alternative approach is to consider the *energy* required to break or uproot a tree. This was attempted by Bartelt and Stöckli (2001), but due to some dubious assumptions in their derivation, we propose an independent evaluation of the effect here. Dorren and Berger (2005) measured the fracture work for a single tree, W_f, by measuring the loss of kinetic energy of rocks when they broke spruce trees, compared these values to results from published laboratory tests on green wood samples, and tested the correlation between breaking energy and maximum bending moment, $M_{b,\,\max}$. They found that (i) a linear relation between W_f and M_b is an acceptable approximation, (ii) obtained a relation between fracture work and breast-height diameter d_{BH} for beech:

$$W_f = 1.6\,\mathrm{MJ\,m^{-2.3}}\, d_{\mathrm{BH}}^{2.3}, \tag{15}$$

and (iii) the coefficient in Eq. (15) can be multiplied with the ratio of the maximum bending moments of another tree species and beech to obtain a satisfactory approximation

for that other species. For 0.2 m < DBH < 0.4 m, the fracture work for a beech tree is in the range 40–200 kJ. This is quite similar to the values from pulling tests obtained by Ribeiro and others (2016). The work for uprooting was of the same order in the Central Amazon basin, but apparently is lower in the Grava dei Bruciati, even though it cannot readily be quantified.

Based on these values, we may roughly estimate the travel distance s of the avalanche front from the moment it impacts the tree until the tree is broken or uprooted: $s \sim W_f/F_t$. For $d_{\mathrm{BH}} = 0.3\,\mathrm{m}$, $\rho_f = 150\,\mathrm{kg\,m^{-3}}$, $h_f = 2\,\mathrm{m}$ and $\bar{u} = 30\,\mathrm{m\,s^{-1}}$, we find $W_f \lesssim 100\,\mathrm{kJ}$, $F_t \sim 40\,\mathrm{kN}$ and $s \lesssim 2.5\,\mathrm{m}$. Since the pressure may be smaller at the very tip of the avalanche, the destruction zone may well be larger, but presumably not much more than perhaps 10 m in a large avalanche. With this, one can express the last term in the numerator of Eq. (13) as $N_t F_t/B \approx W_f n \cos\theta$, with typical values in the range 3–10 $\mathrm{kN\,m^{-1}}$. The first and second term in that equation are of the order of 300–500 $\mathrm{kN\,m^{-1}}$ and thus much larger, but they largely cancel each other.

Turning to Eq. (14), we can assume values in the range $h_{ne} = 0.5$–1 m, $\rho_{sc} \approx 150\,\mathrm{kg\,m^{-3}}$, $n = 0.03$–$0.1\,\mathrm{m^{-2}}$ and $m_t = 2$–4 t. This leads to

$$\begin{aligned} \dot{M}/B &= (\dot{M}_t + \dot{M}_{sc})/B \\ &\sim [(2\text{–}10) + (2\text{–}5)] \cdot 10^3\,\mathrm{kg\,m^{-1}s^{-1}} \\ &\sim (6\text{–}12) \cdot 10^3\,\mathrm{kg\,m^{-1}s^{-1}}. \end{aligned} \tag{16}$$

Writing Eq. (13) with the help of Eq. (14) as

$$\bar{u}_{\mathrm{eq}}^2 = \frac{Mg(\sin\theta - \mu_{\mathrm{eff}}\cos\theta) - N_t F_t}{nm_t + \rho_{sc} h_{ne}}$$

and using the mass estimates from Sec. 4, $M \sim 20$–40 kt, a path width and mean slope angle in the range 100–150 m and 30°, respectively, and an effective friction coefficient of about 0.4, we arrive at

$$\bar{u}_{\mathrm{eq}} \sim 25\text{–}55\,\mathrm{m^{-1}s^{-1}} \tag{17}$$

for the asymptotic avalanche speed when gravity, friction and entrainment are in balance. While the uncertainty is very large, this range is compatible with the speed estimates of Sec. 3. All together, a consistent picture of the main factors determining the dynamics of this avalanche arises.

5.2 Limits from damage to Hotel Rigopiano

Inferences from destruction of buildings The complete destruction of Hotel Rigopiano may provide more substantial lower bounds on the pressure, but only at one location in the path. However, we do not have enough information about the structural strength of the different parts of the hotel complex to make more than an educated guess about the avalanche pressure: From period photos, it seems the original Rifugio Tito Acerbo was

Figure 6 Partial view of the destroyed Hotel Rigopiano. The spa area in the foreground is moderately damaged, but the upper two floors of the old Rifugio Tito Acerbo were annihilated and the four-story main complex collapsed completely and was displaced by some 10 m. Photo from `http://primadanoi.it`*, retrieved on 2017-08-09*

built in masonry, presumably without steel reinforcement. If that is the case, impact pressures in the range 20–50 kPa are expected to be sufficient to destroy the building. When tree trunks transported at roughly the same speed as the avalanche impact the building, the pressure in an area of approx. 0.1 m^3 will reach several megapascal for tens to hundreds of milliseconds. This should be enough to break the mortar between the stones, which typically has a shear strength of the order of several hundred kPa.

Interesting information can be gained from Fig. 6: The photo shows largely unscathed forest in close proximity to the eastern wing of the hotel, the former Rifugion Tito Acerbo. While the perspective of the image may be deceiving, it looks as though the straight continuation of the eastern trimline would cross the building. If correct, this would imply that the avalanche pressure along the trimline was high enough to utterly destroy the old masonry structure.

Inferences from displacement of the hotel The photos give evidence that virtually all of the western, main wing was displaced by at least 10 m in the flow direction of the avalanche. We do not have sufficient information about the failure mode of the ground floor and what degree of shear resistance the joint between the foundation and the hotel walls had. However, a lower bound on the pressure can be obtained by estimating $\bar{p}_f$, the necessary pressure to overcome friction, from A_{impact}, the effective impact area of the avalanche, M_h, the mass of the building, and μ_h, the effective friction coefficient of the house debris on its foundation. Our assumptions with regard to the mass of the

Table 2 Assumptions used for estimating the minimum avalanche impact pressure at the location of the hotel from the friction force of the rubble against the foundation

Object	Count	Length (m)	Width (m)	Height (m)	Density ($\mathrm{kg\,m^{-3}}$)	Mass (t)
Exterior walls long	2	25	0.3	3	2000	90
Exterior walls short	2	12	0.3	3	2000	40
Interior walls long	7	20	0.2	2.5	1200	80
Interior walls short	20	10	0.2	2.5	1200	120
Floors	4	25	12	0.25	1500	450
Roof	1	25	12	0.2	1000	60
Snow on roof	1	25	12	2	250	150
Furniture, etc.						60
Total mass						1050

building are summarized in Table 2; note that these estimates were obtained purely on the basis of photos and have a large degree of uncertainty. The dense or fluidized part of the avalanche probably had a flow depth of 2–3 m, giving an impact area of 25–40 $\mathrm{m^2}$. The friction coefficient of the debris is unknown, but in view of all iron bars and the roughness of fracture surfaces, it certainly was at least 0.5, and perhaps even larger than 1. With this, one obtains a mean avalanche pressure in the range

$$\bar{p}_{\mathrm{av}} \approx \frac{\mu_h M_h g}{A_{\mathrm{impact}}} = 120\text{–}400\,\mathrm{kPa}. \tag{18}$$

This pressure range appears plausible for an avalanche of this size: One expects the velocity to be in the range $\bar{u} = 30\text{–}40\,\mathrm{m\,s^{-1}}$ for an avalanche of this size in the upper run-out zone and after mowing down the forest over a distance of 1 km. At NGI's avalanche test site Ryggfonn in western Norway, pressure and velocity are simultaneously recorded by load plates and Doppler radar, respectively. The measurements on dry-snow avalanches indicate that $C_D\bar{\rho}$ mostly is in the range 80–200 $\mathrm{kg\,m^{-3}}$ (Gauer and others, 2008). The drag coefficient of the load plates is presumably somewhat smaller than that of a large wall such as the backside of the hotel. With $C_D\bar{\rho} \approx 100\text{–}250\,\mathrm{kg\,m^{-3}}$, we obtain an impact pressure

$$\bar{p}_{\mathrm{aval}} = C_D\bar{\rho}\bar{u}^2 = 90\text{–}400\,\mathrm{kPa}, \tag{19}$$

in surprisingly good agreement with the estimate (18)—albeit with very large uncertainties.

6 On the vulnerability of buildings and persons hit by snow avalanches

In quantitative risk assessment, risk is commonly treated as the product of three factors, namely (i) the *hazard* or the probability of a potentially disadvantageous event happening at a given point, (ii) the *exposure* as the number of persons or the value of objects being present when such an event happens, and (iii) the *vulnerability* of persons or objects, expressed as the conditional probability of, e.g., death or critical injury to a person or the probable degree of damage of an object given a hazardous event:

$$R = \sum_S P(S)E(S)V(S), \tag{20}$$

where S represents a specific scenario. For snow avalanches, a scenario can be defined as an avalanche reaching some given point $\mathbf{x}$ with some given pressure p. The summation over S is then replaced by an integral over $\mathbf{x}$ and p and the hazard expressed as the differential probability per unit time, $p\,\mathrm{d}\mathbf{x}\,\mathrm{d}p$.

As discussed by Issler and others (2016b), the vulnerability function $V(S)$ or $V(\mathbf{x}, p)$ is still poorly known, not in the least because it strongly depends on the type of building that is affected by the avalanche. In order to enable use of data on avalanches hitting different types of building, they adopt the working hypothesis that the vulnerability of persons is governed by the degree of damage, D, i.e. how much the building has lost its protective function against avalanches; in other words, $V(D)$ is assumed independent of the type of building. The construction type b determines the degree of damage as a function of impact pressure, $D(p, b)$. It is advantageous to categorize buildings into a number of classes, ranging from wood-frame houses (like the houses typically found in Norway) over wooden block and unreinforced brick houses to reinforced concrete buildings. The degree of damage is a number between 0 and 1 (or between 0% and 100%). Also, different classes of vulnerability may be considered, e.g., the probability of grave injury or death, or the probability of moderate injury.

With regard to the damage function $D(p, b)$, the Rigopiano avalanche can give us the following information:

- The main building can probably be classified as a large multi-story masonry building, whereas the newer spa complex was a one- or two-story reinforced-concrete construction. Neither of them was specifically dimensioned for avalanche impact. Note that these classifications need to be confirmed.
- The impact pressure of the avalanche can only be inferred from numerical simulations, which are fraught with large uncertainties because the initial conditions are poorly known and most models do not explicitly consider fluidization or the formation of a powder snow cloud.

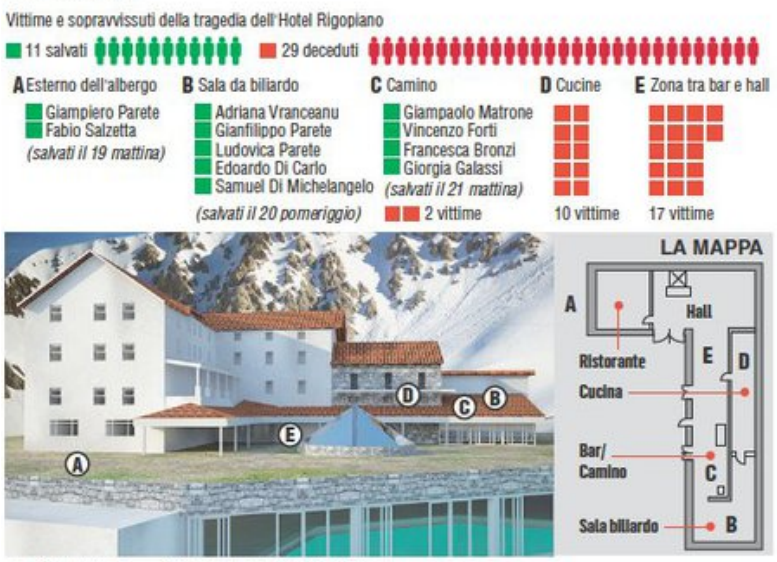

Figure 7 Plan view of the hotel/spa complex and location of the survivors and victims. Modified from https://www.quotidiano.net/cronaca/foto/rigopiano-mappa-vittime-1.2849742, retrieved on 2017-08-09.

Table 3 Categorization of the degree of damage as proposed by Issler and others (2016b)

Degree of damage D		Damage description
Category 1:	0.0–0.1	All spaces intact to slightly skewed. Big voids and structure are stable.
Category 2:	0.1–0.4	Impact side partly pushed in or skewed, limited voids at impact side, big voids at lee side, partly skewed/damaged internal walls. Snow/avalanche debris in 10–20% of the building.
Category 3:	0.4–0.7	Impact side pushed in/collapsed, big voids approx. 50%, small voids due to snow avalanche debris approx. 20%. Snow/avalanche debris in at least 50% of the building.
Category 4:	0.7–0.9	Impact side pushed in/collapsed, internal walls collapsed, no big voids, small voids due to snow avalanche debris approx. 20%. Snow/avalanche debris in at least 90% of the building.
Category 5:	0.9–1.0	All spaces destroyed, (almost) no voids remain, large part of building scattered, most walls destroyed.

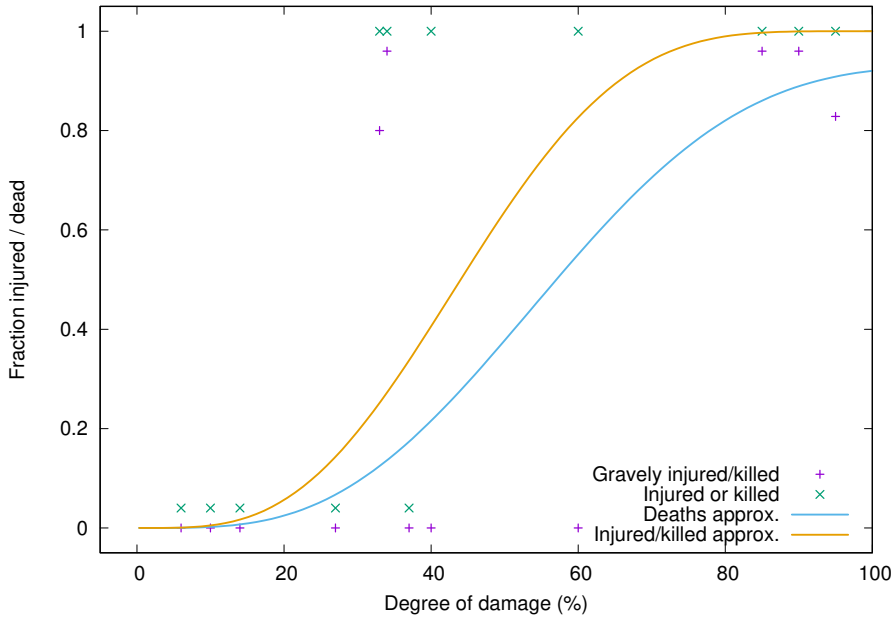

Figure 8 Vulnerability data from the 2015-12-19 Longyearbyen and 2017-01-18 Rigopiano avalanches combined. The data points from Rigopiano are those with $D = 0.6$ (game room) and $D = 0.95$ (hotel lobby). The full curves are only meant to guide the eye; they correspond to $V_{\text{injury}}(D) = I_x(D; 4, 5)$ and $V_{\text{death}}(D) = 0.93 I_x(0.8D; 4, 5)$, respectively, where I_x is the incomplete Beta function. Note that the parameters have been fitted only visually.

- The damage to the main building was in Category 5, $D \approx 1$.
- Images in the media suggest that the spa complex collapsed only partially. Snow entered the building in large quantities and blocked the way for the children in the gaming room, but left them with enough space and air for surviving over an extended period. This points to damage in Category 3 and $D \approx 0.5$.

Generally, the degree of damage corresponds to the expectations, given the type of building and the probable range of impact pressure. More detailed information on the constructional details of the main building and the surface of the spa complex that was exposed to the avalanche impact would be helpful. Also for the assessment of the vulnerability function for persons, the location of, and damage to, the gaming room should be known in more detail.

To the author's knowledge, detailed information about where uninjured, moderately injured and deceased persons were found is not released yet. Aggregating somewhat fuzzy information from media reports on the rescue actions and images of the destroyed hotel, the following is assumed for the time being:

- There were a total of 38 persons inside the hotel complex, while two persons

were in the parking lot outside the devastated area and were unharmed.

- Several children were playing in a room near the spa area, which was less exposed to the avalanche. The degree of damage was presumably in Category 3, i.e., between 0.4 and 0.7, since it took up to four days to rescue some of the children.

- Five of the adults were found alive. In at least two cases, the degree of damage seems to be in Category 4, yet the persons were only lightly injured.

- The death toll was 29 adults who were gathered in the hotel lobby at the time the avalanche struck. As the entire four-story main building was displaced some 10 m and completely collapsed, one can assume the degree of damage to be in Category 4 or 5.

In Fig. 8, these data are combined with those from the 2015-12-19 Longyearbyen (Svalbard) avalanche. In the case of Longyearbyen, each house hit by that avalanche gives rise to two separate data points, one for each story. For Rigopiano, the adult victims apparently were all gathered in the lobby and most of the children in a game room, which were damaged to different degrees. Therefore, the Rigopiano data appears as two separate data points. For each data point from Longyearbyen as well as for the one from the game room at Rigopiano, the "sample size", i.e., the number of persons exposed to the avalanche, was very small (1–5) so that the statistical uncertainty is very large; for this reason, it is not plotted in the figure. The statistical uncertainty of the data points from the Rigopiano lobby, however, is about ± 0.17. The reader should be aware that the lines in the plot are only meant to guide the eye—they are not the result of a rigorous statistical analysis, which does not seem to be warranted yet. The trends from this limited data set can be summarized as follows:

- The data for damage in Categories 4 and 5 appear quite consistent between the Longyearbyen and Rigopiano events. Somewhat surprisingly, six persons out of 35 survived building damage of degree 5 in Rigopiano, despite the long time it took to find and free them.

- Within the statistical uncertainty, the data from the Rigopiano game room is also consistent with the findings from Longyearbyen, even though the three children in Rigopiano may have survived essentially unscathed in a quite severely damaged room. The degree of damage should, however be reassessed once more detailed information is released.

7 Conclusions

The observations on the 2017 Rigopiano avalanche described in [I] were limited by the short duration of the survey and the inaccessibility of the surroundings of the hotel ruins. Nevertheless, many interesting aspects of the dynamics of this event could be analyzed on the basis of this data, using simple yet physically based descriptions. We summarize the main findings:

- Among the four avalanches that occurred in the vicinity of Rigopiano around January 18, 2017, the Grava dei Bruciati avalanche was the only one that ran beyond the β-point; it even passed the α-point.
- The estimated front speeds in the range 25–40 m $^{-1}$ have a wide margin of uncertainty, but are of the same order as observations, measurements and numerical simulations of avalanches of similar size. The slow-moving, dense parts of the avalanche appear to have moved at about half the speed of the front. This agrees with observations and analyses in small-to-medium size avalanche paths in the Swiss Alps (Issler and others, 2008).
- Estimates of the mass balance are also fraught with large uncertainties, but a consistent picture emerges. It is probable that a large part of the snow cover was eroded but only partially entrained into the flow. Tree debris contributed as much or more to the mass growth of the avalanche as the snow cover did. The erosion rates (snow and trees) are so high that they were much more of a limiting factor for the velocity than the velocity-dependent part of the normal friction.
- The observed damage patterns are consistent with the pressure estimates derived from the velocity estimates, both with respect to the destroyed forest and the obliterated and displaced hotel. We agree with the earlier conclusions of Bartelt and Stöckli (2001) that the breaking or uprooting of the entire forest does not significantly decelerate the avalanche, in contrast to the decelerating effect of entrainment. The destruction front was probably a short zone shortly behind the avalanche front.
- When expressed as a function of the degree of building damage, the lethality curve resulting from the Rigopiano event was consistent with the one found in the 2015 Longyearbyen avalanche within the large uncertainties due to the small statistical base. This confirms the usefulness of the degree of damage as the proper variable for obtaining a universal relation that does not depend on the building type.

The analyses presented here also provide a few pointers for future work. The first is that simple mechanical considerations often allow one to deduce a considerable amount of semi-quantitative information from limited observational information. Each inference

has a large margin of uncertainty, but if they all are consistent with each other, the probability of them being far off will be small. Thus analysis of a large number of such observations can provide valuable insight on issues of avalanche dynamics, e.g., their scaling behavior or the conditions and frequency of specific flow regimes occurring.

The collected data can be used for detailed tests of dynamical avalanche models, as already attempted by, e.g., Frigo and others (2018). When more observational data is hopefully released after the conclusion of the court case, one may hope that the initial and boundary conditions (among others the probable release area and release depth, the snow density, the mass balance and the forest density and tree size) can be specified with more certainty. NGI plans to test the code MoT-Voellmy, which can account for both entrainment and extra flow resistance due to a forest stand. However, from the analysis in Sec. 5.1 one concludes that the braking effect of the forest stand is overestimated by a factor of 10–100 if uprooting and/or breaking are not included. On the other hand, the entrainment of tree debris induces significant extra deceleration. It remains to be seen to which extent these two antagonist effects compensate each other.

Some locals of Rigopiano have considerable knowledge about the avalanche history of the area, including release frequency and run-out distance in many avalanche paths on the eastern flank of this mountain chain. If these observations could be collected, critically analyzed, compared with a detailed dendrochronological study as presented by, e.g., (Favillier and others, 2017), and supplemented by numerical simulations, high-quality avalanche hazard maps could be elaborated for this little studied, rather southerly area. Such a map is presently missing and would contribute towards a solid and safe basis for the future touristic development of the surroundings of Farindola, which has suffered an enormous set-back from this tragic event.

Acknowledgements

Alessia Errera and Massimiliano Barbolini furnished valuable information about the event, the rescue operations and the coverage in the Italian media as well as about the forensic investigations (still ongoing as this report is being written) and their consequent restrictions of the field work. Jan-Thomas Fischer shared the notes of a survey by an Austrian team during the rescue operations. Thomas Scrine played a pivotal role at Farindola by pointing out that the access restrictions were less severe than the office at the municipality claimed and brought the author in contact with Daniele Borgheggiani, who provided a good map of the area, suggested a safe itinerary and provided important information about avalanche activity around Rigopiano. I sincerely thank them all for their invaluable support of this work. I am also grateful for the valuable comments on the manuscript I received from my colleagues at NGI, most notably … Funding for this work came from the Norwegian Department of Oil and Energy through the grant to NGI for avalanche research (project 20170131 SP4 FoU Snøskred), administrated by the Directorate of Waterways and Energy (NVE).

References

Bartelt P and Stöckli V (2001) The influence of tree and branch fracture, overturning and debris entrainment on snow avalanche flow. *Annals Glaciol.*, **32**, 209–216 (doi: 10.3189/172756401781819544)

Chehata D, Zenit R and Wassgren CR (2003) Dense granular flow around an immersed cylinder. *Phys. Fluids*, **15**(6), 1522–1531 (doi: 10.1063/1.1571826)

Dorren LKA and Berger F (2005) Stem breakage of trees and energy dissipation during rockfall impacts. *Tree Physiol.*, **26**(1), 63–71

Favillier A, Guillet S, Morel P, Corona C, Lopez Saez J, Eckert N, Ballesteros Cánovas JA, Peiry JL and Stoffel M (2017) Disentangling the impacts of exogenous disturbances on forest stands to assess multi-centennial tree-ring reconstructions of avalanche activity in the upper Goms Valley (Canton of Valais, Switzerland). *Quat. Geochronol.*, **42**, 89–104 (doi: 10.1016/j.quageo.2017.09.001)

Forest Products Laboratory (1999) Wood handbook. wood as an engineering material. General Technical Report FPL-GTR-113, Forest Products Laboratory, Forest Service, U.S. Dept. of Agriculture, Madison, Wisconsin

Frigo B, Chiaia B, Chiambretti I, Bartelt P, Maggioni M and Freppaz M (2018) The January 18th 2017 Rigopiano disaster in Italy – analysis of the avalanche dynamics. In *Proc. Intl. Snow Science Workshop, Innsbruck, Austria, 2018*, 6–10, International Snow Science Workshop

Gauer P, Lied K and Kristensen K (2008) On avalanche measurements at the Norwegian full-scale test-site Ryggfonn. *Cold Regions Sci. Technol.*, **51**, 138–155 (doi: 10.1016/j.coldregions.2007.05.005)

Issler D (2018) Field survey of the 2017 Rigopiano avalanche. NGI Technical Note 20170131-02-TN, Norwegian Geotechnical Institute, Oslo, Norway

Issler D, Errera A, Priano S, Gubler H, Teufen B and Krummenacher B (2008) Inferences on Flow Mechanisms From Snow Avalanche Deposits. *Annals Glaciol.*, **49**(1), 187–192 (doi: 10.3189/172756408787814915)

Issler D, Gauer P, Schaer M and Keller S (2016a) Field observations on three mixed snow avalanches, submitted for publication as Supplementary Materials

Issler D, Jónsson Á, Gauer P and Domaas U (2016b) Vulnerability of houses and persons under avalanche impact – the avalanche at Longyearbyen on 2015-12-19. In *Proceedings of the Intl. Snow Science Workshop ISSW 2016, Breckenridge, Colorado*, 371–378, International Snow Science Workshop

Issler D, Gauer P, Gleditsch Gisnås K and Domaas U (2019) Approaches to including climate and forest effects in avalanche hazard indication maps in Norway. *(to be submitted)*

Lied K and Bakkehøi S (1980) Empirical calculations of snow-avalanche run-out distance based on topographic parameters. *J. Glaciol.*, **26**(94), 165–177

Lied K and Toppe R (1989) Calculation of maximum snow-avalanche run-out. *Annals Glaciol.*, **13**, 164–169

Mattheck C, Bethge K, Kappel R, Mueller P and Tesari I (2003) Failure modes for trees and erlated criteria. In B Ruck, C Kottmeier, C Mattheck, C Quine and G Wilhelm (eds.), *Proc. Intl. Conf. 'Wind Effects on Trees', Karlsruhe, Germany*, P9/1, Laboratory

of Building and Environmental Aerodynamics, Institute for Hydromechanics, University of Karlsruhe, Karlsruhe, Germany, iSBN 3-00-011922-1

Ribeiro GHPM, Chambers JQ, Peterson CJ, Trumbore SE, Magnabosco Marra D, Wirth C, Cannon JB, Négron-Juárez RI, Lima AJN, de Paula EVCM, Santos J and Higuchi N (2016) Mechanical vulnerability and resistance to snapping and uprooting for Central Amazon tree species. *Forest Ecol. Mgmt.*, **380**, 1–10 (doi: 10.1016/j.foreco.2016.08.039)

Sovilla B, Sommavilla F and Tomaselli A (2001) Measurements of mass balance in dense snow avalanche events. *Annals Glaciol.*, **32**, 230–236

Takeuchi Y, Nishimura K and Patra A (2018) Observations and numerical simulations of the braking effect of forests on large-scale avalanches. *Annals Glaciol.*, **59**(77)

Wassgren CR, Cordova JA, Zenit R and Karion A (2003) Dilute granular flow around an immersed cylinder. *Phys. Fluids*, **15**(11) (doi: 10.1063/1.1608937)

Kontroll- og referanseside / Review and reference page

Dokumentinformasjon/*Document information*		
Dokumenttittel/*Document title* Dynamical Aspects of the 2017 Rigopiano Avalanche		**Dokumentnr./*Document no.*** 20170131-08-TN
Dokumenttype/*Type of document* Teknisk notat / *Technical note*	**Oppdragsgiver/*Client*** Norges vassdrags- og energidirektorat	**Dato/*Date*** 2019-01-21
Rettigheter til dokumentet iht kontrakt/*Proprietary rights to the document according to contract* ÅPEN: Skal tilgjengeliggjøres i åpent arkiv (BRAGE) / *OPEN: To be published in open archives (BRAGE)*		**Rev.nr. & dato/*Rev.no. & date*** 0 / 2019-01-21
Emneord/*Keywords* Snow avalanche dynamics, forest damage, historic events, Rigopiano		

Stedfesting/*Geographical information*	
Land, fylke/*Country* Abruzzo (Italy)	**Havområde/*Offshore area*** —
Kommune/*Municipality* Farindola	**Feltnavn/*Field name*** —
Sted/*Location* Rigopiano	**Sted/*Location*** —
Kartblad/*Map* 140 II-NO (Castelli), series 25v	**Felt, blokknr./*Field, Block No.*** —
UTM-koordinater/*UTM coordinates* **Sone:** 33N **Øst:** 399 850 **Nord:** 4 698 380	**Koordinater/*Coordinates*** **Projeksjon, datum:** — **Øst:** ° ’ ” **Nord:** ° ’ ”

Dokumentkontroll/*Document control*
Kvalitetssikring i henhold til/*Quality assurance according to* NS-EN ISO9001

Rev.	**Revisjonsgrunnlag/*Reason for revision***	**Egenkontroll av/*Self review by:***	**Sidemanns-kontroll av/ *Colleague review by:***	**Uavhengig kontroll av/ *Independent review by:***	**Tverrfaglig kontroll av/ *Interdisciplinary review by:***
0	Originaldokument	Dieter Issler			

Dokument godkjent for utsendelse / *Document approved for release*	**Dato/*Date***	**Prosjektleder/*Project Manager***
	…	Frode Sandersen

NGI (Norges Geotekniske Institutt) er et internasjonalt ledende senter for forskning og rådgivning innen ingeniørrelaterte geofag. Vi tilbyr ekspertise om jord, berg og snø og deres påvirkning på miljøet, konstruksjoner og anlegg, og hvordan jord og berg kan benyttes som byggegrunn og byggemateriale.

Vi arbeider i følgende markeder: Offshore energi – Bygg, anlegg og samferdsel – Naturfare – Miljøteknologi.

NGI er en privat næringsdrivende stiftelse med kontor og laboratorier i Oslo, avdelingskontor i Trondheim og datterselskap i Houston, Texas, USA og i Perth, Western Australia.

www.ngi.no

NGI (Norwegian Geotechnical Institute) is a leading international centre for research and consulting within the geosciences. NGI develops optimum solutions for society and offers expertise on the behaviour of soil, rock and snow and their interaction with the natural and built environment.

NGI works within the following sectors: Offshore energy – Building, Construction and Transportation – Natural Hazards – Environmental Engineering.

NGI is a private foundation with office and laboratory in Oslo, branch office in Trondheim and daughter companies in Houston, Texas, USA and in Perth, Western Australia.

www.ngi.no

OSLO
TRONDHEIM
HOUSTON
PERTH

NORGES GEOTEKNISKE INSTITUTT
NGI.NO

Hovedkontor Oslo
PB. 3930 Ullevål Stadion
0806 Oslo

Avd. Trondheim
PB. 5687 Sluppen
7485 Trondheim

T 22 02 30 00
F 22 23 04 48
NGI@ngi.no

BANK
KONTO 5096 05 01281
ORG.NR. 958 254 318MVA

ISO 9001/14001
CERTIFIED BY BSI
FS 32989 / EMS 612006